

# Lizardite–chrysotile veins from Vempalle Formation of Cuddapah Supergroup, India: a study in fluid–rock interaction

Kasturi Chakraborty<sup>1,\*</sup>, Praveer Pankaj<sup>2</sup>, Prabir Kumar Mukhopadhyay<sup>3</sup> and Sandip Nandy<sup>4</sup>

<sup>1</sup>Geological Survey of India, Khanij Bhavan, Jaipur 302 004, India

<sup>2</sup>Geological Survey of India, Seminary Hills, Nagpur 440 006, India

<sup>3</sup>AD-18/5, Sector-I, Salt Lake City, Kolkata 700 064, India

<sup>4</sup>Geological Survey of India, Dharitri Building, Sector V, Salt Lake City, Kolkata 700 091, India

**Much work has been done on hydrothermal alteration and serpentinization of high-magnesian bulks like dunite or peridotite. In contrast, serpentinization of dolomite has received scant attention. In this study we focus on a system of nearly monomineralic intersecting veins comprising serpentine or epidote or calcite developed within Vempalle dolomite of unmetamorphosed Cuddapah Supergroup of rocks, Eastern Dharwar Craton, India. Our studies show that hydrothermal alteration under moderately low temperature, low pressure and moderate silica activity can lead to extensive serpentinization of the dolomitic host. Development of talc can occur under increased silica activity at similar  $P$ – $T$  conditions. We also explore the mechanism of formation of chrysotile veins, epidote veins and calcite veins that transect the lizardite which replaces dolomite.**

**Keywords:** Dolomite, fluid–rock interaction, lizardite and chrysotile veins, silica activity.

THE three commonly occurring polymorphs of serpentine are lizardite, chrysotile and antigorite. The first two are low-temperature polymorphs frequently occurring together in the same environment. Lizardite is volumetrically the most abundant serpentine that stabilizes at temperatures below  $\sim 300^\circ\text{C}$ . Field, isotopic and laboratory evidence are in agreement in characterizing antigorite as the high-temperature form of Mg-serpentine, corresponding to formation temperatures  $\geq 250^\circ\text{C}$  (refs 1–3). Oxygen-isotope thermometry-based  $P$ – $T$  diagram shows a stable field for chrysotile between  $195^\circ\text{C}$  and  $260^\circ\text{C}$ , with lizardite stable below and antigorite above this temperature range<sup>1,2</sup>. However, lizardite and chrysotile frequently occur together, particularly in retrograde metamorphosed (hydrated) peridotites<sup>3</sup>. Also, the difference in their Gibbs free energies is not more than 2 kJ in the  $300$ – $400^\circ\text{C}$  range. Above  $\sim 300^\circ\text{C}$ , antigorite + brucite is more stable than

both. In other words, chrysotile is not the most stable form of serpentine. A reasonable explanation is that relative stability of chrysotile and lizardite in nature is determined not by temperature but by kinetic factors or fluid saturation that favours one over the other under different circumstances<sup>3–5</sup>.

A number of asbestos mines operating in Pulivendla region, Andhra Pradesh, India exploit the serpentine mineralization developed at the contact of mafic sills and Vempalle dolomite. A network of serpentine (both lizardite and chrysotile), talc, epidote and calcite veins transects both the lithologies. Much work has been done on the serpentine formation in altered/retrograde metamorphosed peridotites. Nearly pure magnesian end-member lizardite and chrysotile (99%  $\text{Mg}_3\text{Si}_2\text{O}_5(\text{OH})_4$ ) have been studied in magnesian marbles<sup>6–8</sup>. However, a comprehensive study on their development in dolomite is relatively scarce in the literature<sup>3,9–15</sup>. The present work explores serpentine formation in unmetamorphosed dolomitic rocks and the role of fluid therein.

## Regional geology

The Proterozoic Cuddapah Supergroup unconformably overlies the older granites and greenstone belts of the Eastern Dharwar Craton. The Cuddapah basin exposes a thick sequence of terrigenous and chemogenic sedimentary rocks with a comparatively minor fraction of igneous rocks in the form of lava flows, sills, dykes and plugs (Figure 1). King<sup>16</sup> proposed the first ever account of Cuddapah stratigraphy, followed by significant developments by subsequent workers<sup>17</sup>. Extensive geophysical data available on Cuddapahs, especially on western Cuddapahs, prove the presence of a massive elliptical gravity high below this part of the basin (Figure 1c)<sup>18</sup>. The geophysical anomaly has been generally attributed to a small mantle plume that was active below the southwestern part of the Cuddapah basin during the Palaeoproterozoic<sup>18,19</sup>. Chakraborty *et al.*<sup>20</sup> correlated the mafic magmatism,

\*For correspondence. (e-mail: kasturigs@gmail.com)

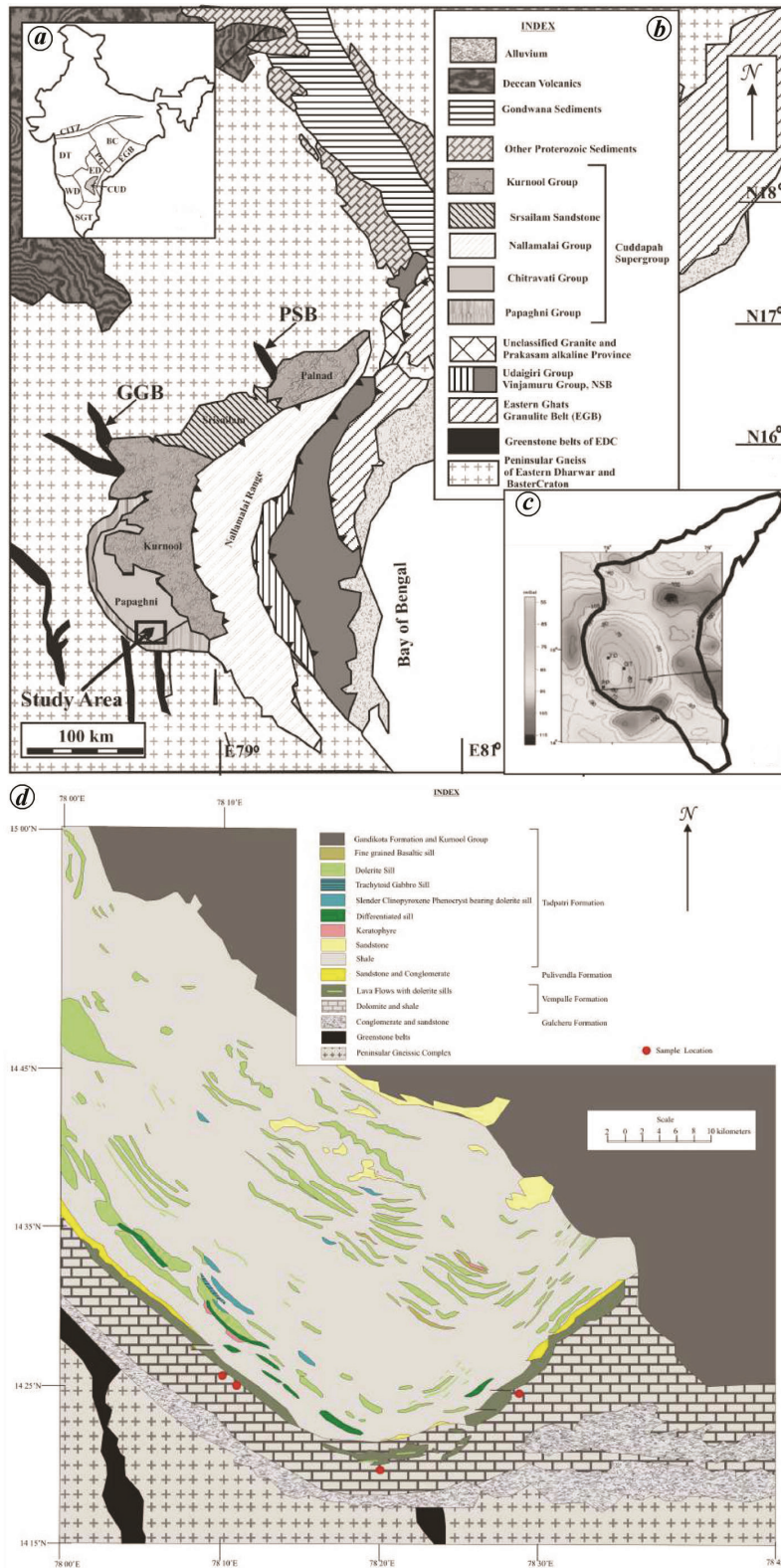


**Figure 1.** *a*, Inset map showing the position of Cuddapah Basin in the South Indian Craton. *b*, Geological map of different sub-basins within the Cuddapah Basin in Eastern Dharwar Craton (modified after Geological and mineral map of Andhra Pradesh (2005), Saha *et al.*<sup>30</sup>; Geological Survey of India, Misc. Pub. No. 30 (ref. 32); Tripathy and Saha<sup>33</sup>). *c*, Geophysical map of Cuddapah Basin showing gravity high below southwestern Cuddapah (after Chandrakala *et al.*<sup>18</sup>). *d*, Geological map of a portion of the Cuddapah Basin showing Vempalle dolomite and the overlying mafic lava flows. The sills in Vempalle are mostly subsurface and can be accessed within mines. Sample locations for serpentinite have been marked with red-filled circles (map from Geological and mineral map of Andhra Pradesh (2005) and Saha *et al.*<sup>31</sup>, Geological Survey of India, Misc. Pub. No. 30 (ref. 32) and modified after the present study).

including volcanism and emplacement of sills within sediments in the western Cuddapah basin with incipient crustal rifting, possibly triggered by plume-related mantle upwelling, high heat flow and crustal thinning.

The undeformed and unmetamorphosed Vempalle Formation in the Papagani sub-basin of lower Cuddapahs is constituted of over 1000 m thick dolomite, limestone, chert breccias, shale, siliceous oolite and minor quartzite (Figure 1 *d*). Mafic sills and lava flows dominate the stratigraphy in the uppermost part of the Formation (Figure 1 *d*). Individual flows are altered and epidotized. Angular clasts of sedimentary rocks, including chert, jasper and stromatolitic dolomite along with fragments of pillowed basalts within the Vempalle lava suggest explosive submarine eruption<sup>20</sup>. Barite occurs as disjoint lenses within the Vempalle Formation.

### *Serpentine veins of the Vempalle Formation*

Srikantia<sup>21</sup> reported basic sills from the uppermost Vempalle Formation in areas west of Erraguntla and north of

Vempalle town. During our studies, we encountered dolerite sills of variable thickness in Sogalpalli as well as in Bakkanagarpalle and Midipenta. These concordant intrusive bodies are generally medium to fine-grained with an occasional quartz-filled vesicle, suggesting shallow level emplacement in the accumulating sediment pile. Asbestos mineralization is associated with mafic sills of the Vempalle Formation<sup>21</sup>. The present study examined the dolerite sills at the contact of dolomite at Brahmanapalle and Ippatla that have developed serpentine and talc at both the contacts with adjoining dolomite. These serpentinized horizons at present can only be studied in underground mine sections (Figure 2 *a*). Green, yellowish-green and greenish-white coloured serpentine are presently mined from this area (Figure 2 *b*). Veins of serpentine of varying thickness transect both dolomite and dolerite sills at the contact of the two lithotypes (Figure 2 *c* and *d*). Remnant lenses of host rock are often preserved within the veins (Figure 2 *c*). The serpentine in the more massive veins is generally very fine-grained aggregate and is cross-cut by numerous monomineralic centimetre to millimeter-thick veins of fibrous chrysotile asbestos, fibrous calcite or fine-grained epidote (Figure 2 *c–e*).

### **Petrography and mineral chemistry**

#### *Veins of the Vempalle Formation*

The veins at the contact of mafic sills and dolomite of the Vempalle Formation are predominantly serpentine (lizardite and chrysotile), although near-monomineralic epidote, talc and calcite veins were also noted. Serpentine is generally very fine-grained to platy lizardite transected by veins of coarser platy chrysotile (Figure 2 *e*; Figure 3 *a* and *b*). The fibres of chrysotile are generally oriented at high angle to the vein walls, with fibres from both sides meeting along a more or less symmetric midline (Figure 2 *e*). Remnant lenses of dolomite are frequently present within lizardite or chrysotile (Figure 3 *a*). Veins of fibrous calcite growing at high angle to the vein wall cross-cut the lizardite and chrysotile veins, often with remnant serpentine within the veins (Figure 3 *c*). Veins of epidote and talc have developed only at the immediate contact of dolerite with the adjoining carbonate layer.

Micro-Raman spectrometry proves to be a useful characterization tool for resolving structural differences at the scale of the grain, in cases where multiple polymorphs of serpentine are present that prove to be optically difficult to distinguish. Micro-Raman study of the serpentine veins was carried out using a micro-Raman spectrometer (Renishaw In-Via Reflex) at the Geological Survey of India (GSI), Kolkata. The device is fitted with a diode laser operating at 785 nm, and spectral resolution of 1 cm<sup>-1</sup>. A confocal microscope (Leica) is used to focus the laser on the sample, using objective lenses of 20×, 50× and 100×



**Figure 2.** *a*, Serpentinized veins in underground mine section. *b*, Mined-out green, yellowish-green and greenish-white coloured serpentine. *c*, Hand specimen showing vein of serpentine in dolomite. Note the lobes of serpentine replacing dolomite. *d*, Hand specimen showing thin veins of chrysotile within dolerite sill. *e*, Hand specimen showing lizardite vein in dolomite with fibrous chrysotile vein in lizardite.

magnification. The microscope is equipped with binoculars and a software-interactive video camera, allowing precise positioning of the sample and selecting a specific region for study. The 514 nm argon laser (2400 lines/mm grating) could only be occasionally used due to high fluorescence of the rock. The backscattered light passes through a holographic notch filter (HNF), which rejects the abundant elastic Rayleigh scattering, to avoid outshining of the weaker Raman signal. The backscattered light is dispersed using a 1200 lines/mm grating and is detected on a Peltier-cooled CCD-detector. This configuration was used to collect data in the spectral region between 100 and 3690  $\text{cm}^{-1}$ . Spot-beam diameter was varied from 0.84 to 1.2  $\mu\text{m}$  and focus energy was between 15 and 18 mW. Accumulation time was generally 50 sec, but was occasionally increased to 100–150 sec. Such scan times and accumulation numbers were chosen to provide adequate signal-to-noise ratios. Figures 4 and 5 present typical Raman spectra of the phases. The spectral resolution for each Raman vibrational mode is in the order of  $\pm 1\text{--}2 \text{ cm}^{-1}$ .

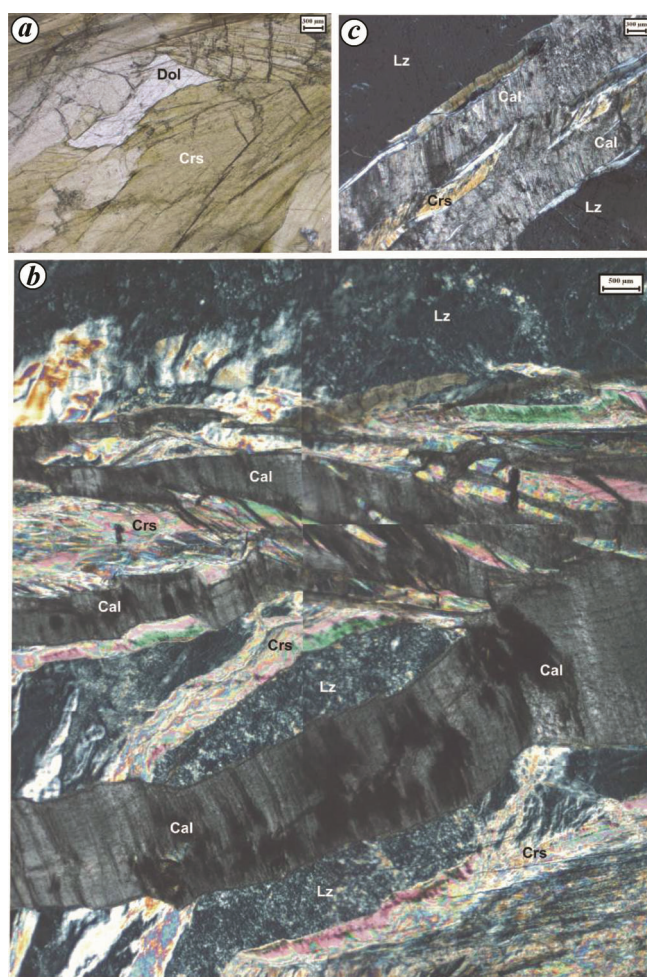


**Figure 3.** *a*, Remnant dolomite within chrysotile (PPL). *b*, Irregular chrysotile veins transecting lizardite and fibrous calcite veins cutting across chrysotile veins (XPL). *c*, Calcite vein within lizardite. The calcite is fibrous and grows at a high angle to the vein wall. Note the chrysotile grains within the calcitic vein (XPL).

Before and after each analysis, any shift in the Raman peak position related to spectrometer drift was corrected using the first-order Raman band peak position of a silicon wafer that ideally exhibits a peak at 520.7  $\text{cm}^{-1}$ . The in-built Wire 3.4 software was used to perform the background correction before each Raman band was fitted to an in-built mineral library for identification. Finally, each corrected spectrum was compared with the RRUFF project database<sup>22</sup> and the serpentine database of Groppo *et al.*<sup>23</sup> to identify the phases.

The minerals that could be identified or confirmed using Raman spectroscopy are lizardite, chrysotile, dolomite inclusions within chrysotile, calcite in veins, epidote in veins, talc and dusty graphite (Figures 4 and 5). Lizardite was distinguished from chrysotile on the position of the  $\text{Mg}(\text{O}, \text{OH})_6$  group vibrations whose characteristic peaks for antigorite are in the range  $\sim 197\text{--}202 \text{ cm}^{-1}$ , while the same is  $\sim 195\text{--}197 \text{ cm}^{-1}$  for lizardite and  $\sim 191\text{--}193 \text{ cm}^{-1}$  for chrysotile<sup>23</sup>. Also variations exist in the peak positions of  $\nu_s \text{ Si-O}_b\text{-Si}$  which is in the range 688–692  $\text{cm}^{-1}$  for lizardite, 693–694  $\text{cm}^{-1}$  for chrysotile and 683–684  $\text{cm}^{-1}$  for antigorite. The Si–O asymmetric vibration band at 1090–1094  $\text{cm}^{-1}$  for lizardite and at 1102–1110  $\text{cm}^{-1}$  for chrysotile could be detected in many samples. None of the samples showed the characteristic Si–O–Si stretching band at around 1045  $\text{cm}^{-1}$  that typically characterizes antigorite. Also, no sample showed the characteristic peaks of 279 and 440  $\text{cm}^{-1}$  which appear in brucite along with all the typical peaks of lizardite. Only one sample of lizardite had an additional peak at 282  $\text{cm}^{-1}$ , which possibly does not characterize brucite. Thus brucite can be conclusively eliminated from the possibility of being interwoven with lizardite. Table 1 presents a representative set of sample analyses.

Phase chemical analyses were carried out using electron probe micro analyser (CEMECA SX100) at the EPMA Laboratory, GSI, Kolkata. The instrument was operated at 15 kV accelerating voltage and 20 nA beam current. The beam size was kept at  $\sim 1 \mu\text{m}$  for all analyses. Natural mineral standards were used for all the elements and PAP correction was applied. Tables 2 and 3 present the representative mineral compositions. Compositional data indicate that Mg (2.82–2.86 apfu) and Fe (0.02–0.04 apfu) are present as the major octahedral cations within lizardite, defining an  $\sim X_{\text{Mg}}$  value of  $\sim 0.98\text{--}0.99$ . Al and Cr atoms per formula unit are negligible (Table 2). Epidote grains from the monomineralic epidote veins are Ca- and Fe-rich (Table 2). Table 2 also presents calcite analysis from the calcite fibre veins.

### *Dolomite adjoining the serpentine veins*

The dolomitic rocks at the contact of sills are white or grey to buff-coloured and fine-grained in the hand specimen, and are frequently stromatolytic (Figure 6*a*). The

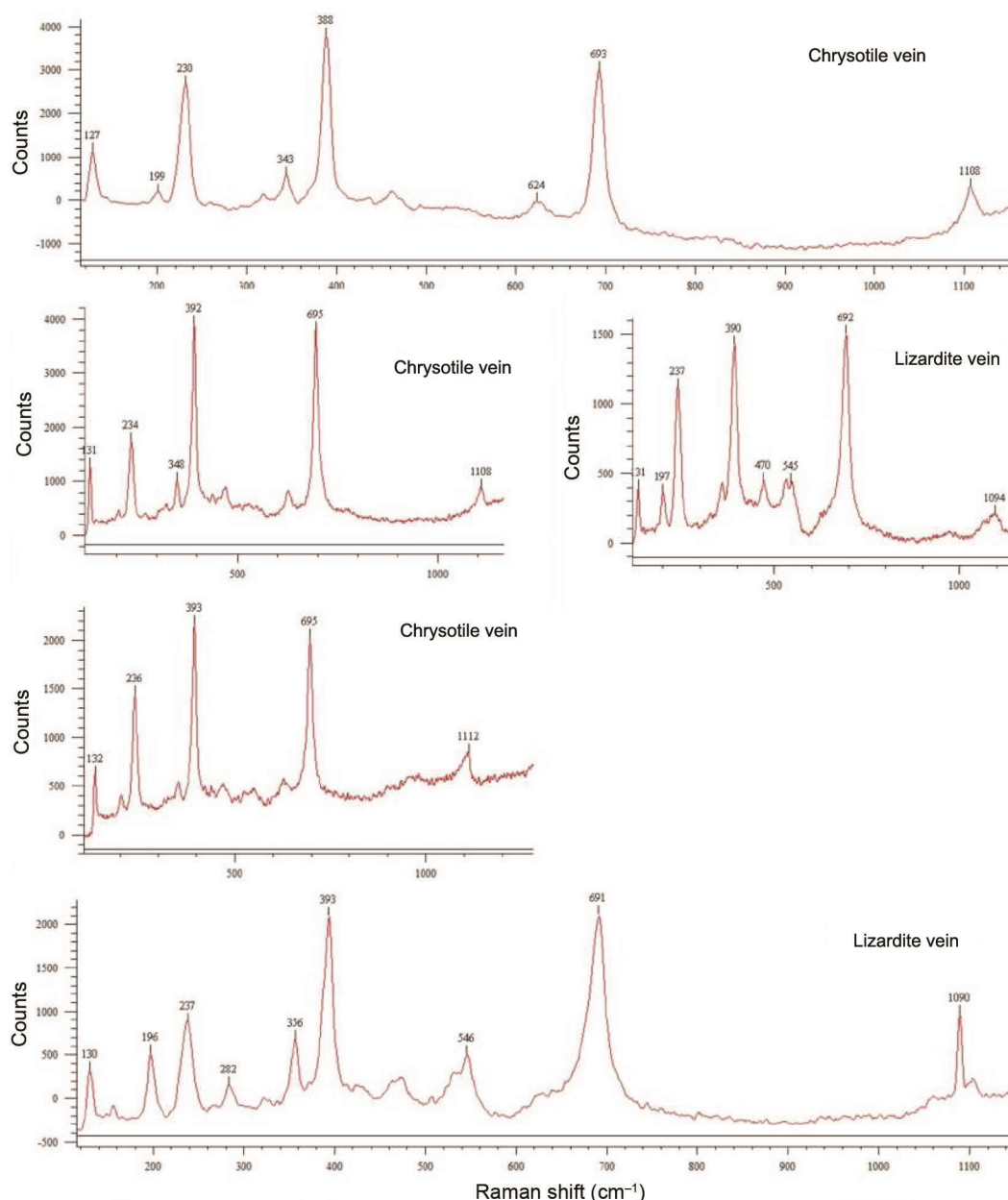


**Figure 4.** Laser Raman spectroscopic profiles of serpentine grains from the veins.

proportion of dolomite to calcite is normally very high. However, in the dolomite at the immediate contacts of intrusive sills, where abundant serpentine veins have developed, alizarin red S staining technique helps in the identification of coarser nodules of calcite within the otherwise fine-grained dolomite (Figure 6 b).

#### *Dolerite sills*

The sills intercalated with Vempalle lava flows are medium-grained and consist of extensively chloritized clinopyroxene and partially carbonatized plagioclase along with medium-grained skeletal magnetite (Figure 6 c and d).

Epidote has developed profusely in these rocks. Although altered, the igneous texture can be easily discerned as intergranular to subophitic. At present, mostly fine-grained chlorite fills the spaces between prismatic sub-hedral plagioclase grains. Remnant clinopyroxene within the fine-grained chlorite has compositions in the range  $\sim\text{En}_{15-34}\text{Fs}_{17-37}\text{Wo}_{29-50}$  (Table 3), while plagioclase is strongly albitic ( $X_{\text{Ab}} \sim 0.94-0.95$ ; Table 3). Major portions of the plagioclase grains are carbonatized (Figure 6 c-d). The Na-enrichment in remnant plagioclase can therefore be arguably ascribed to preferential partitioning of Ca in the carbonate that partially replaces these grains. Many of the sills contain small quartz and chlorite-filled vesicles. Fine

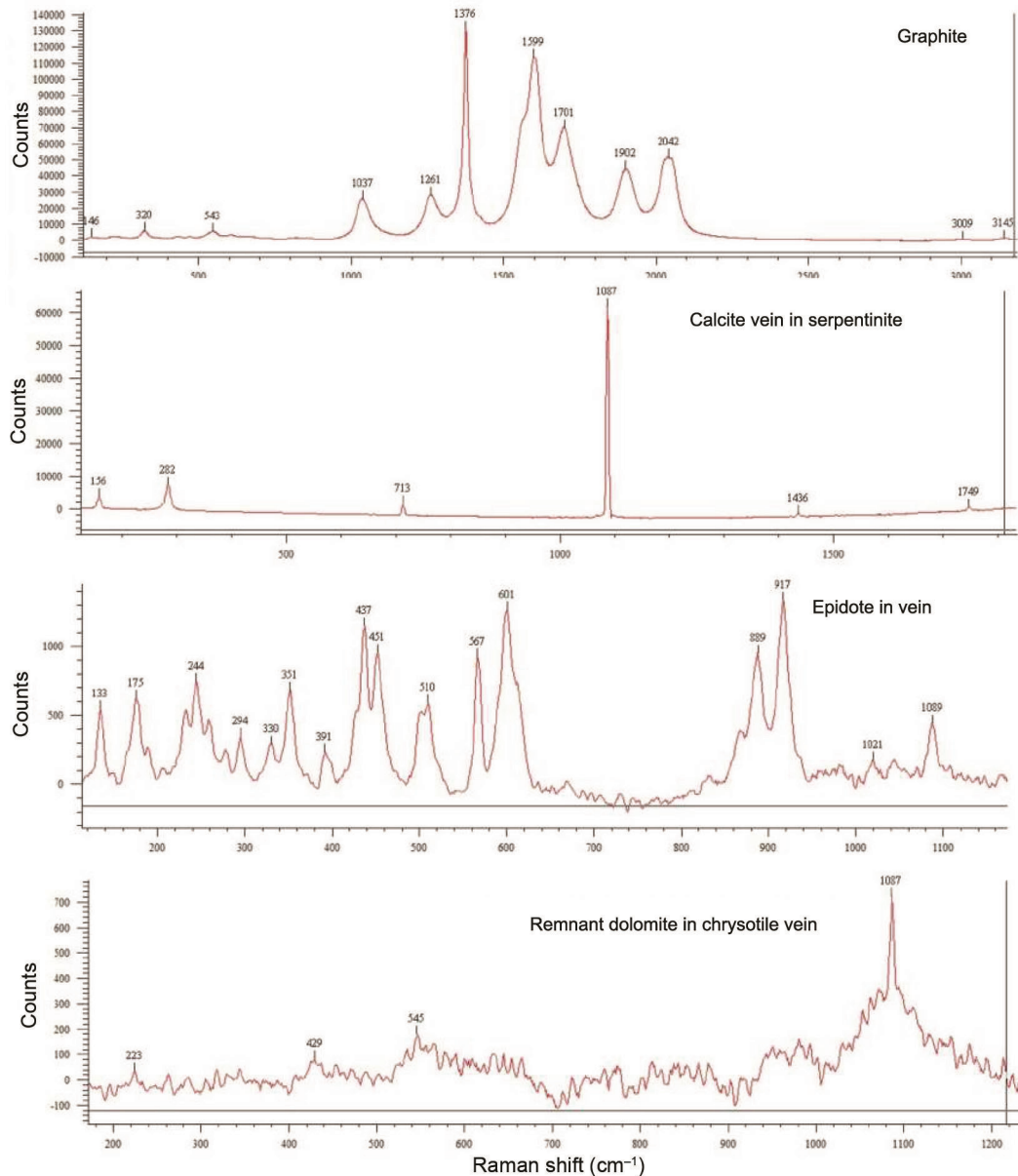


**Figure 5.** Laser Raman spectroscopic profiles of graphite, calcite, epidote and dolomite from the veins of Vempalle Formation.

epidote veins transect these rocks near their contacts with adjoining serpentinite.

## Discussion

### *P–T conditions for serpentinitization of dolomite: a study from phase relations*

In the absence of suitable geothermometers, the phase assemblages in the veins and adjoining rocks have been studied to estimate the temperature of serpentine formation. Development of epidote veins alongside serpentine, chloritization, epidotization and carbonatization of the sills as well as the overlying lava flows, rare occurrence

of actinolite partially replacing clinopyroxene in the sills and presence of amygdular epidote, chlorite, quartz and calcite in the mafic lava flows suggest temperature in sub-greenschist to lower greenschist facies (Figure 6 c–f).

Stable serpentine polymorphs in the veins are lizardite and chrysotile. Antigorite is conspicuously absent. In a comprehensive study, Evans<sup>3</sup> concluded that chrysotile has no stability field and the relative stability of chrysotile over its polymorph lizardite is dependent on factors like abundance of fluid, supersaturation and availability of open pore spaces. Accordingly, the MSH phase diagram of Evans<sup>3</sup>, reproduced in Figure 7, precludes any chrysotile stability field and limits lizardite to temperatures less than 350°C (ref. 3). Likewise, our  $T-X_{\text{SiO}_2}$



**Table 3.** Representative clinopyroxene and plagioclase compositions from the mafic sills of Vempalle Formation

| Formation sample               | Vempalle sill PV-140 |               |          |          |          |          | Vempalle sill PV-48 |         |
|--------------------------------|----------------------|---------------|----------|----------|----------|----------|---------------------|---------|
|                                | Cpx 1 October        | Cpx 1 October | Cpx 14/1 | Cpx 17/1 | Cpx 18/1 | Cpx 30/1 | PI 27/1             | PI 30/1 |
| SiO <sub>2</sub>               | 49.53                | 49.53         | 50.36    | 49.31    | 49.13    | 52.53    | 67.33               | 68.15   |
| TiO <sub>2</sub>               | 0.74                 | 0.74          | 0.73     | 0.61     | 0.72     | 0.42     | 0.01                | 0.00    |
| Al <sub>2</sub> O <sub>3</sub> | 1.79                 | 1.79          | 1.70     | 1.17     | 2.00     | 1.57     | 19.57               | 19.75   |
| Cr <sub>2</sub> O <sub>3</sub> | 0.02                 | 0.02          | 0.02     | 0.05     | 0.03     | 0.16     | 0.00                | 0.00    |
| FeO                            | 15.74                | 15.74         | 15.99    | 19.20    | 14.57    | 10.39    | 0.13                | 0.15    |
| MnO                            | 0.31                 | 0.31          | 0.30     | 0.37     | 0.30     | 0.26     | 0.00                | 0.00    |
| MgO                            | 12.98                | 12.98         | 12.28    | 12.16    | 13.43    | 16.50    | 0.00                | 0.00    |
| CaO                            | 17.21                | 17.21         | 18.39    | 16.10    | 18.34    | 17.43    | 0.97                | 1.15    |
| Na <sub>2</sub> O              | 0.22                 | 0.22          | 0.24     | 0.17     | 0.24     | 0.16     | 10.97               | 11.03   |
| K <sub>2</sub> O               | 0.00                 | 0.00          | 0.01     | 0.03     | 0.00     | 0.03     | 0.08                | 0.08    |
| NiO                            | 0.04                 | 0.04          | 0.00     | 0.00     | 0.03     | 0.01     | 0.04                | 0.00    |
| Total                          | 98.57                | 98.57         | 100.00   | 99.17    | 98.77    | 99.45    | 99.10               | 100.31  |
| Si                             | 1.92                 | 1.92          | 1.93     | 1.93     | 1.90     | 1.96     | 2.97                | 2.97    |
| Ti                             | 0.02                 | 0.02          | 0.02     | 0.02     | 0.02     | 0.01     | 0.00                | 0.00    |
| Al                             | 0.08                 | 0.08          | 0.08     | 0.05     | 0.09     | 0.07     | 1.02                | 1.02    |
| Cr                             | 0.00                 | 0.00          | 0.00     | 0.00     | 0.00     | 0.00     | 0.00                | 0.00    |
| Fe                             | 0.51                 | 0.51          | 0.51     | 0.63     | 0.47     | 0.32     | 0.00                | 0.01    |
| Mn                             | 0.01                 | 0.01          | 0.01     | 0.01     | 0.01     | 0.01     | 0.00                | 0.00    |
| Mg                             | 0.75                 | 0.75          | 0.70     | 0.71     | 0.77     | 0.92     | 0.00                | 0.00    |
| Ca                             | 0.71                 | 0.71          | 0.75     | 0.67     | 0.76     | 0.70     | 0.05                | 0.05    |
| Na                             | 0.02                 | 0.02          | 0.02     | 0.01     | 0.02     | 0.01     | 0.94                | 0.93    |
| K                              | 0.00                 | 0.00          | 0.00     | 0.00     | 0.00     | 0.00     | 0.00                | 0.00    |
| Ni                             | 0.00                 | 0.00          | 0.00     | 0.00     | 0.00     | 0.00     | 0.00                | 0.00    |
| #Cation                        | 4.03                 | 4.03          | 4.02     | 4.04     | 4.04     | 4.00     | 4.99                | 4.99    |
| X(Mg)                          | 0.38                 | 0.38          | 0.35     | 0.35     | 0.38     | 0.47     |                     |         |
| En                             | 0.38                 | 0.38          | 0.36     | 0.35     | 0.39     | 0.47     |                     |         |
| Fs                             | 0.26                 | 0.26          | 0.26     | 0.31     | 0.24     | 0.17     |                     |         |
| Wo                             | 0.36                 | 0.36          | 0.38     | 0.34     | 0.38     | 0.36     |                     |         |
| X <sub>An</sub>                |                      |               |          |          |          |          | 0.05                | 0.05    |
| X <sub>ab</sub>                |                      |               |          |          |          |          | 0.95                | 0.94    |
| X <sub>or</sub>                |                      |               |          |          |          |          | 0.00                | 0.00    |

diagram, prepared with the updated thermodynamic dataset of Holland and Powell<sup>24</sup> using PERPLEX 6.6.8 at  $X_{\text{CO}_2} \sim 0.001$  and  $P = 3$  kbar, suggests a limited stability field for lizardite below 200°C and entirely eliminates any chrysotile stability field<sup>25</sup>. Increase in  $X_{\text{CO}_2}$  values does not change the scenario. In contrast, several workers have confirmed the survival of both lizardite and chrysotile at temperatures in excess of 400°C (ref. 3). Thus, the currently available thermodynamic dataset cannot be conclusively used for determining the  $P$ – $T$  conditions based strictly on the serpentine polymorph.

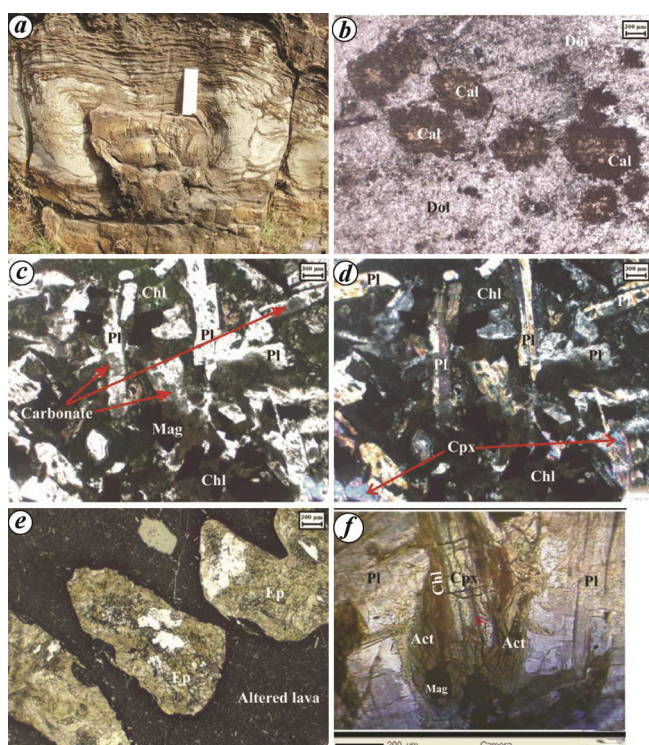
The veins of Vempalle, while rich in serpentine (lizardite/chrysotile), calcite and remnant dolomite, generally lack talc and tremolite. These serpentine veins directly replace the dolomitic host rock (Figure 2 *c* and *e*). Figure 8 *a* is a  $T$ – $X_{\text{CO}_2}$  diagram in the CMSV system, constructed using the dataset of Holland and Powell<sup>24</sup> that allows stability of dolomite + serpentine assemblage in a wide range of  $X_{\text{CO}_2}$  values at temperatures below 350–400°C at 1 kbar pressure. Above this temperature, talc should stabilize in the system – a phase that was generally absent in Vempalle dolomite, except locally in the immediate contact of the intrusive dolerites. Also there is a general up-temperature expansion of the serpentine stability field towards water-rich conditions. Figure 8 *b* elaborates the red box in

Figure 8 *a*, with extreme water-rich phase equilibria that preferentially stabilize serpentine to higher temperature. Even under such aqueous conditions, the reaction: dolomite + quartz  $\rightarrow$  talc + calcite limits the serpentine + dolomite assemblage to temperatures below  $\sim 250^\circ\text{C}$  in a pressure range 1–3 bar. Note that a general term ‘Serp’ representing any polymorph of serpentine has been used in the diagrams. This is because while thermodynamic calculations predict antigorite stability, the phase observed in our studies is lizardite. The possible reasons for such apparent contradiction have been discussed later in the article. With no direct geothermometric data, the mineralization temperature for the veins of the Vempalle Formation can be conservatively estimated as  $<300^\circ\text{C}$  from phase equilibrium calculations.

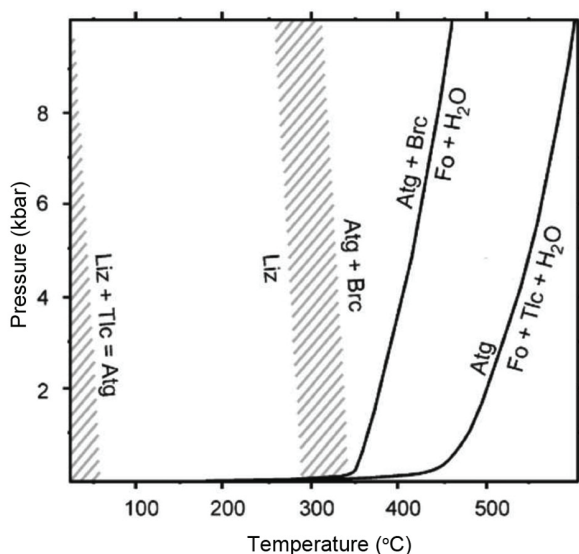
Based on the similarity of composition of the mafic sills to the overlying lava flows, the occasional presence of amygdules within the sills and occurrence of stromatolites in the host dolomite, it can be reasonably concluded that the magma was emplaced at a very shallow depth and was possibly the feeder to the overlying flows. Thus the ambient pressure was not more than 1–3 kbar.

Figure 8 *c* presents the  $T$ – $X_{\text{CO}_2}$  diagram at a higher pressure of 3 kbar. A comparative study with Figure 8 *a* suggests that although the serpentine-absent invariant shifts

to lower  $X_{CO_2}$  values with the rise in pressure, the overall serpentine stability field remains largely pressure-insensitive. Further increase of pressure stabilizes aragonite, which has not been observed in the system.



**Figure 6.** *a*, Stromatolytic structure in dolomitic marble. *b*, Recrystallized coarser calcite on fine-grained dolomite adjoining serpentine veins – the pink colour in calcite is due to alizarin red S treatment. *c*, Altered dolerite sill showing relict intergranular texture and patchy carbonatization of plagioclase laths (PPL). *d*, Altered dolerite sill showing relict intergranular texture with remnant clinopyroxene and plagioclase (XPL). *e*, Altered mafic lava with amygdular epidote and carbonate. *f*, Corona of actinolite on clinopyroxene in dolerite sill.



**Figure 7.** Stability fields of lizardite and antigorite in pressure–temperature field (from Evans<sup>3</sup>).

It can therefore be reasonably inferred that the  $P$ – $T$  condition of vein formation was  $\leq 3$  kbar and  $< 300^\circ\text{C}$ . As the Vempalle Group of rocks is generally an unmetamorphosed stack of supracrustals, such lower greenschist to sub-greenschist facies condition must have been attained only very locally in the immediate vicinity of the sills due to thermal flux from the cooling magma.

### Control of silica activity and fluid on serpentinization

Serpentinization of pure dolomite requires addition of both silica and  $\text{H}_2\text{O}$  to the system. The vein-type serpentinization within the Vempalle dolomite indicates that such additive components were accessed through channelized fluid flow. The effect of silica on dolomitic host has been demonstrated in the  $T$ – $a_{\text{SiO}_2}$  diagram (Figure 9*a*). Constructed with the software PERPLEX 6.6.8 based on Connolly *et al.*<sup>25</sup> and using updated thermodynamic data from Holland and Powell<sup>24</sup>, Figure 9*a* shows the relation between phases in the CMSV system (CaO–MgO–SiO<sub>2</sub>–fluid) under varying temperatures and silica activity. Serpentine (antigorite specifically) has a wide stability field over a large range of silica activity up to a maximum temperature limit of  $500^\circ\text{C}$  at 3 kbar pressure under extreme  $\text{H}_2\text{O}$  enrichment ( $X_{\text{CO}_2} \sim 0.001$ ). Very high silica activity stabilizes talc at the cost of serpentine. General absence of the later phase from the studied veins suggests moderate silica activity at temperatures around  $300^\circ\text{C}$  under hydrous conditions. However, local occurrence of talc at the immediate contact of dolerite sills was possible due to a higher silica gradient from the altering pyroxene in dolerite.

Increase in  $X_{\text{CO}_2}$  enlarges the stability fields of dolomite and calcite. This effectively shifts the reactions towards higher temperature and silica activity (white arrows in Figure 9*a*). In contrast, further decrease in  $\text{CO}_2$  concentration expands the stability of antigorite to temperatures  $\leq 300^\circ\text{C}$ . Thus fluid composition as well as silica activity have played vital roles in determining the stability of serpentine minerals within Vempalle dolomite.

Figure 9*b* is an isothermal–isobaric  $a_{\text{SiO}_2}$  –  $X_{\text{CO}_2}$  plot in the CMSV system at  $300^\circ\text{C}$  and 3 kbar. The invariant point at  $X_{\text{CO}_2} \sim 0.38$  limits direct serpentine development from dolomite in the absence of talc to a water-rich environment. Also, the breakdown of serpentine to tremolite through the reaction calcite + serp → tremolite, restricts serpentine stabilization from dolomite to a narrow silica activity range ( $\log a_{\text{SiO}_2} \sim -1$ ). Decrease in temperature shifts the invariant point towards lower  $X_{\text{CO}_2}$  (white arrow in Figure 9*a*), effectively increasing the stability of talc and restricting that of serpentine towards increasingly water-rich conditions.

The phase relations suggest that serpentinization of dolomite in the Vempalle Formation took place at  $< 300^\circ\text{C}$  and

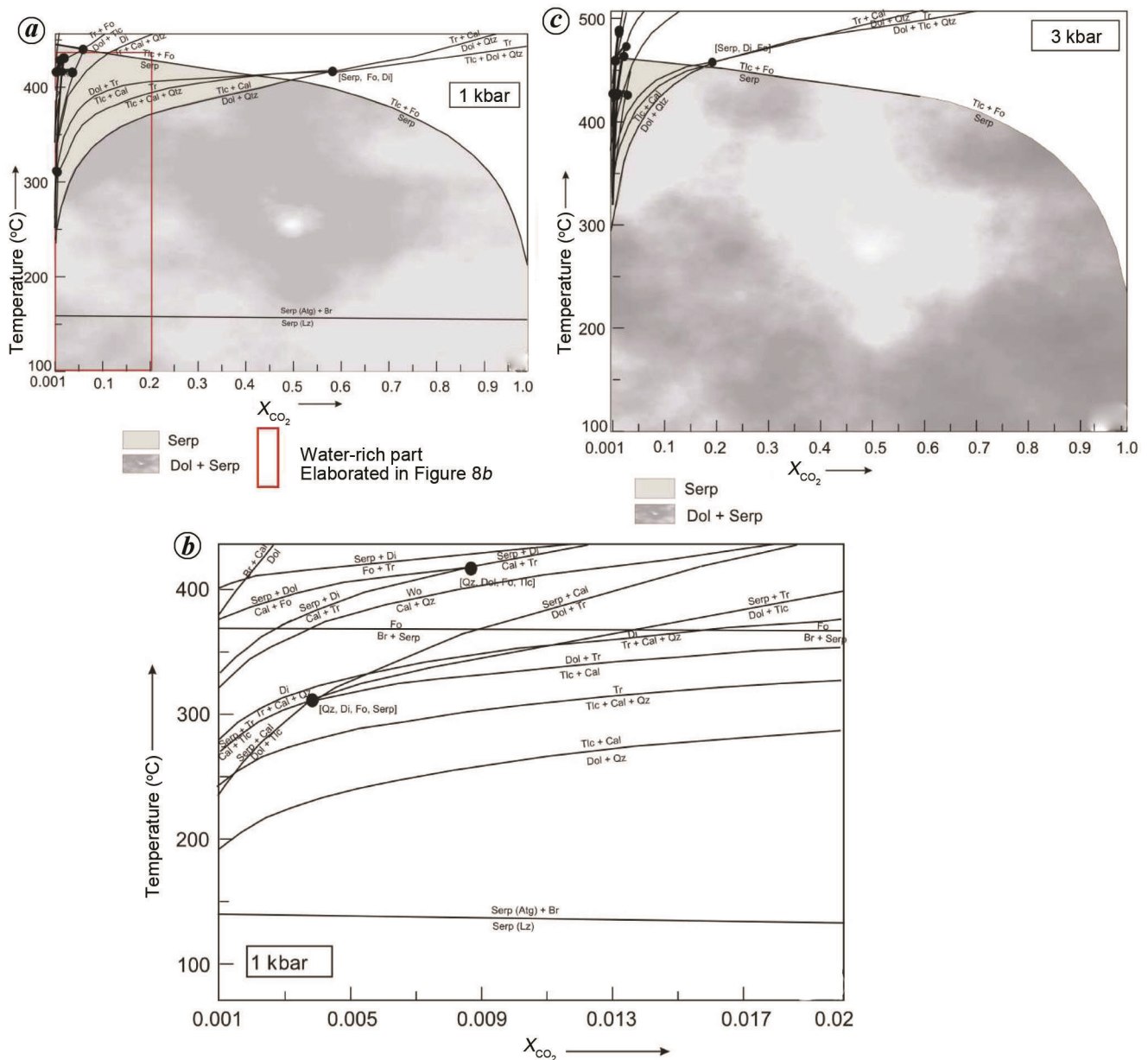


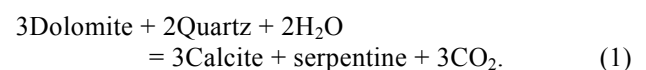
**Figure 8.** *a*, Isobaric  $T-X_{CO_2}$  diagram at 1 kbar showing stability field of dolomite (Dol) + serpentine (Serp) assemblage in the CMSV system. *b*,  $T-X_{CO_2}$  diagram elaborating the highly aqueous end of (a) (red box). *c*, Isobaric  $T-X_{CO_2}$  diagram at 3 kbar showing stability field of dolomite + serpentine assemblage in the CMSV system.

$\leq 3$  kbar under dominantly hydrous conditions and moderate silica activity.

#### Phase relations and development of lizardite and talc veins

Field study in Vempalle dolomite shows that the serpentine veins directly replace the host rock without development of talc or tremolite (Figure 2 *a*, *c* and *e*). Remnant dolomite lenses were noted within serpentine during petrographic analyses (Figure 3 *a*). Not only was the serpentine interlaced by fibrous calcite veins (Figure 3 *b-c*),

but coarser calcite replacing dolomite was also observed in the surrounding host rock (Figure 4 *b*). Our observations thus suggest the following serpentine and calcite-forming reaction



The black arrow in Figure 9 *a* shows the reaction at 300–400°C at moderate silica activity and hydrous conditions. The reaction can proceed to the right either through a rise in temperature or in silica activity, or both. Subsequent

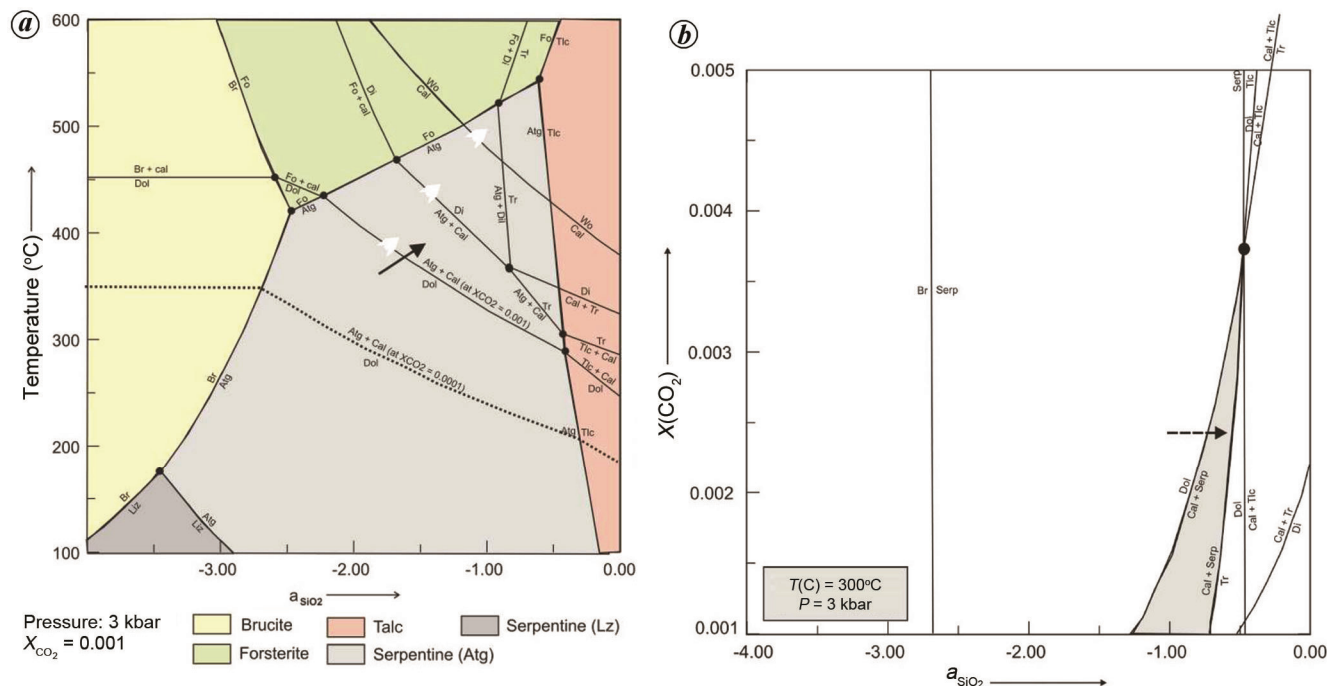
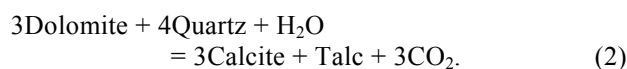


**Figure 9.** *a*, Isobaric  $T$ - $a_{\text{SiO}_2}$  diagram at  $X_{\text{CO}_2} \sim 0.001$  and 3 kbar pressure. The phase relations show stability ranges of lizardite, antigorite and talc under varying silica activity. Black arrow represents reaction (1) which can proceed due to rise in temperature or in silica activity, or both. White arrows represent direction of shift of the univariant reactions with rise in  $X_{\text{CO}_2}$ , whereas the dotted line represents reaction (1) under extremely aqueous condition. *b*, Isothermal-isobaric  $X_{\text{CO}_2}$ - $a_{\text{SiO}_2}$  diagram showing stability field of serpentine. Black arrow demonstrates that progression of reaction (1) is more likely through increase in silica activity than a change of  $\text{CO}_2$  percentage in the ambient fluid.

breakdown of serpentine to diopside strictly limits the stability field of serpentine + dolomite + calcite within a narrow temperature range. With further decrease in  $X_{\text{CO}_2}$  the stability field of serpentine expands enabling the reaction to occur at temperatures  $< 300^\circ\text{C}$  (dotted line in Figure 9a). The serpentine thus formed was restricted to the channels of fluid movement within dolomite, thereby forming serpentine veins of varying width.

The stable serpentine polymorph with lowest Gibb’s free energy predicted from the equilibrium equation is antigorite. Lizardite is stabilized only in a restricted field at higher  $X_{\text{H}_2\text{O}}$ -lower silica-low temperature conditions (Figure 9a). However, the phases observed during petrographic analyses were lizardite and chrysotile (Figure 5). Remnant dolomite lenses within lizardite or chrysotile and complete absence of antigorite suggest that these phases have developed directly from dolomite breakdown. Figure 9a shows that in an open system with large amounts of pure  $\text{H}_2\text{O}$  flux, reaction (1) will shift to lower temperatures towards the lizardite stability field. Under such a situation, other stabilizing factors like crystal structure, surface free energy or small quantities of other elements in the system may have expanded the lizardite stability range, so that reaction (1) produces lizardite directly instead of antigorite. This will be in confirmation with observations made by several other workers studying natural systems, where lizardite or chrysotile exists at temperatures in excess of  $400^\circ\text{C}$  (ref. 3).

Talc veins are restricted to the immediate vicinity of the mafic sills. Figure 9a indicates that talc formation from dolomite can be achieved under identical  $P$ - $T$  conditions as that of reaction (1), if only the silica activity is higher in the domain. The talc-forming reaction under such situation is as follows



Thus, only variation in silica can decide between serpentine or talc-rich assemblages developed over small distances.

### Development of chrysotile veins

Chrysotile veins transect the thicker mass of fine-grained lizardite in the studied rocks (Figures 2e, 3b and 5). Textural relation thus shows that chrysotile formation slightly post-dates serpentinization (lizardification) of dolomite.

Laboratory studies and thermodynamic calculations indicate that lizardite is more stable in the MSH system, while chrysotile is a metastable phase. Chrysotile commonly grows as vein-filling cross-fibre and slip-fibre<sup>3</sup>. At nanoscale, chrysotile may be seen to fill voids formed by the deformation of host lizardite<sup>3</sup>. While the Gibb’s free energy values of lizardite and chrysotile are not significantly different, extant studies confirm that chrysotile

requires open space/pore space and a small degree of supersaturation for growth as this particular polymorph cannot exert force of crystallization, except parallel to its C-axis<sup>3,4</sup>.

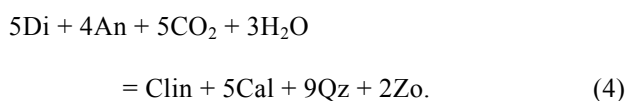
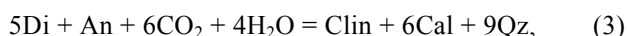
In our studied veins, the preferential growth of lizardite can be attributed to the capacity of the mineral to exert a force of crystallization. Lack of significant pore space at the initiation of the reaction possibly favoured lizardite structure over chrysotile. However, progression of reaction (1) to the right involves  $\Delta v = -21.73 \text{ cm}^3$ , i.e. a decrease in bulk volume assuming the infiltrated fluid completely moves out of the system. If the product calcite is also removed in aqueous solution as  $\text{Ca}^{2+}$  and  $\text{HCO}_3^-$ , then  $\Delta v$  rises to  $-131 \text{ cm}^3$  (molar volume data from Mincrust database; <http://database.iem.ac.ru/mincryst>)<sup>26</sup>. Such reduction in volume will lead to significant space development in the rock in the form of pores or cracks, thereby allowing further fluid permeation and conditions conducive for chrysotile crystallization/recrystallization from the existing lizardite.

#### *Development of epidote veins and source of silica*

Epidotization or epidote veins are known to occur in varied low-temperature geological settings like obducted ophiolites, skarns, propylitic altered mafic volcanics, in late-stage veins related to silicic intrusions, along hydrothermally altered shear zones and from active geothermal systems<sup>27</sup>.

The dolerite sills and overlying mafic lavas of the Vempalle Formation are highly altered with extensive chloritization, carbonatization, epidotization and rare development of actinolite, which suggests sub-greenschist to greenschist facies metamorphism in the presence of binary  $\text{H}_2\text{O}-\text{CO}_2$  fluid (Figure 4 c-f). As the Cuddapah Supergroup is in general unmetamorphosed, such local extensive alteration must have been related to magma emplacement-related higher thermal flux and therefore occurred contemporaneously with igneous activity. A number of thin epidote veins transect the altered sills and are particularly common close to the serpentinite veins. Figure 6 presents the laser Raman spectrum of such an epidote grain.

The CMASV ( $\text{CaO}-\text{MgO}-\text{Al}_2\text{O}_3-\text{SiO}_2$ -fluid) reactions that can lead to the development of chlorite + epidote + carbonate assemblage from clinopyroxene and plagioclase are as follows



While  $\text{CO}_2$  required for these reactions could have been provided by the serpentinitizing dolomite, reactions (3) and (4) produce  $\text{SiO}_2$  which is a necessary component for

prograde serpentine or talc development. The carbonate thus formed through plagioclase breakdown acts as a localized carbon sink, thereby decreasing the concentration of dissolved carbonate/bicarbonate in the permeating fluid (Figure 4 c and d). Very local remobilization of alumina in the permeating fluid along with more easily mobilized  $\text{Ca}^{2+}$  and  $\text{Fe}^{+2}$  led to the formation of the epidote veins.

#### *Development of calcite veins*

Monomineralic veins with brown, fibrous, calcite grains at a high angle to the vein walls cut across both lizardite and chrysotile veins (Figure 3 b and c). Remnant lenses of serpentine often persist within these veins (Figure 3 b and c). This makes calcite veins the latest stage of hydrothermal veining in the serpentinitized Vempalle dolomite.

Both reactions (1) and (2) produce calcite. Solubility of calcite in the ambient fluid depends largely on its pH. At low acid concentration, calcite dissociates in the fluid as  $\text{CaCO}_3 + \text{H}^+ = \text{Ca}^{2+} + \text{HCO}_3^-$ , thus keeping the reaction products  $\text{Ca}^{2+}$  and  $\text{HCO}_3^-$  in solution.

Precipitation of calcite from the veins, although common in nature, is more difficult to explain. As is well known from modern oceans, fall in temperature should increase calcium carbonate solubility. However, loss of acidity of the solution, development of alkalinity or reducing conditions favour calcite precipitation<sup>8,28-30</sup>. Consumption of  $\text{CO}_2/\text{HCO}_3^-$  during carbonatization of plagioclase in reactions (3) and (4) could have acted as the local carbon sink, thereby decreasing acidity of the circulating fluids. That a reducing ambience was attained in the calcite veins could be confirmed from Raman spectroscopic identification of fine-grained graphite associated with calcite (Figure 6). How the reducing condition was created is a matter of speculation in absence of isotopic data. REE signature of the serpentine + calcite veins matches well with the adjoining altered mafic rocks (Figure 10). Absence of negative cerium anomaly precludes active participation of oxygenated seawater. High-temperature dissociation of algal mats in the adjoining carbonates could have contributed further reducing conditions (Figure 4 a). Also, deposition of calcite within a vein requires slightly supersaturated fluid with respect to the components<sup>28</sup>. Such conditions could have been easily achieved within small domains as reaction (1) or (2) proceeded to the right and more  $\text{H}_2\text{O}$  was consumed in serpentinitization.

#### **Conclusion**

Serpentinization of high-magnesian bulks like dunite or peridotite has been well studied. However, dolomitic rocks, another potentially Mg-rich bulk received scant attention. This study shows that serpentinitization of dolomite without

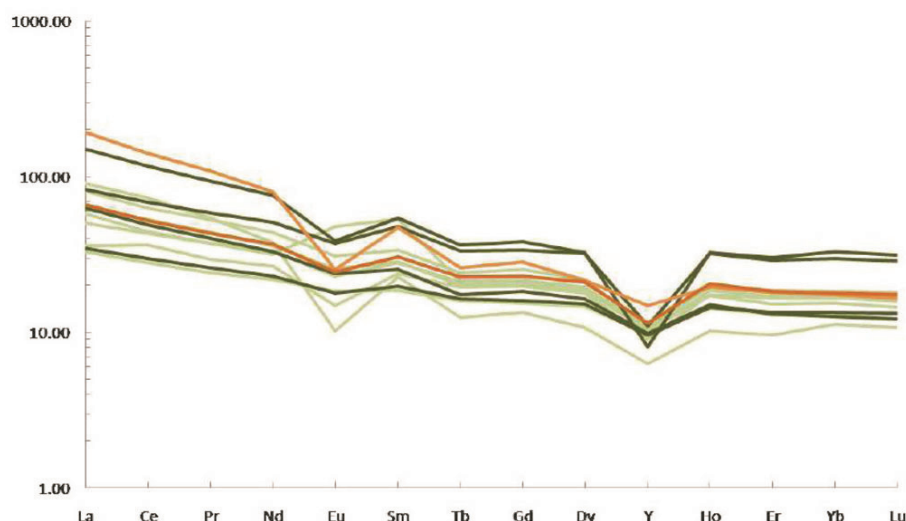


**Figure 10.** Chondrite normalized REE distribution plot for Vempalle lava (pale green), dolerite sills (dark green) and serpentine veins (orange).

development of talc and tremolite can be achieved under a restricted set of conditions which include low temperature ( $\leq 300^{\circ}\text{C}$ ), low pressure ( $< 3$  kbar), extremely water-rich fluid and only moderate silica activity. The study also explores the possible variability in mineral assemblage with variations in fluid composition or silica activity. Thus under higher silica activity, talc-rich veins are expected in identical  $P$ - $T$  conditions. Also, fluid composition plays a major role in the stabilization of serpentine. Epidote veins in the complex had formed through leaching of clinopyroxene and plagioclase in the adjoining dolerite sills. The calcite veins were the last to develop when the circulating fluid gradually became oversaturated with respect to calcium carbonate and possibly also evolved a higher pH.

1. O'Hanley, D. S. and Wicks, J. F., Conditions of formation of lizardite, chrysotile, and antigorite, Cassiar, British Columbia. *Can. Mineral.*, 1995, **33**, 753–774.
2. O'Hanley D. S., *Serpentinites: Records of Tectonic and Petrologic History*, Oxford University Press, Oxford, UK, 1996, p. 277.
3. Evans, B. W., The serpentinite multisystem revisited: chrysotile is metastable. *Int. Geol. Rev.*, 2004, **46**, 479–506.
4. Normand, C., Williams-Jones, A. E., Martin, R. F. and Vali, H., Hydrothermal alteration of olivine in a flow-through autoclave: nucleation and growth of serpentine phases. *Am. Mineral.*, 2002, **87**, 1699–1709.
5. Berman, R. G., Engi, M., Greenwood, H. J. and Brown, T. H., Derivation of internally consistent thermodynamic data by the technique of mathematical programming; a review with application to the system  $\text{MgO-SiO}_2\text{-H}_2\text{O}$ . *J. Petrol.*, 1986, **27**, 1331–1364.
6. Wicks, F. J. and Plant, A. G., Electron-microprobe and X-ray-microbeam studies of serpentine textures. *Can. Mineral.*, 1979, **17**, 785–830.
7. O'Hanley, D. S. and Dyar, M. D., The composition of lizardite 1T and the formation of magnetite in serpentinites. *Am. Mineral.*, 1993, **78**, 391–404.
8. Nagy, B. and Faust, G. T., Serpentes: natural mixtures of chrysotile and antigorite. *Am. Mineral.*, 1956, **41**, 817–838.

9. Dungan, M. A., Metastability in serpentine-olivine equilibria. *Am. Mineral.*, 1977, **62**, 1018–1029.
10. Evans, B. W., Metamorphism of alpine peridotite and serpentinite. *Annu. Rev. Earth Planet. Sci.*, 1977, **5**, 397–447.
11. Frost, B. R. and Beard, J. S., On silica activity and serpentinization. *J. Petrol.*, 2007, **48**, 1351–1368.
12. Evans, B. W., Control of the products of serpentinization by the Fe-Mg exchange potential of olivine and orthopyroxene. *J. Petrol.*, 2008, **49**, 1873–1887.
13. Evans, B. W., Lizardite versus antigorite serpentinite: magnetite, hydrogen and life(?). *Geology*, 2010, **38**, 879–882.
14. Plumper, O., Piazzolo, S. and Austrheim, H., Olivine pseudomorphs after serpentinized orthopyroxene record transient oceanic lithospheric mantle dehydration (Leka ophiolite complex, Norway). *J. Petrol.*, 2012, **53**, 1943–1968.
15. Majumdar, A. S., Hovelmann, J., Vollmer, C., Berndt, J., Mondal, S. K. and Putnis, A., Formation of Mg-rich olivine pseudomorphs in Serpentinized Dunite from the Mesoarchean Nuasahi Massif, eastern India: insights into the evolution of fluid composition at the mineral-fluid interface. *J. Petrol.*, 2015, **57**(1), 3–26; doi: 10.1093/petrology/egv070.
16. King, W., The Kadapah and Karnul Formations in the Madras Presidency. *Mem. Geol. Surv. India*, 1872, **8**(1), 1–346.
17. Lakshminarayan, G., Bhattacharjee, S. and Naidu, R., Sedimentation and stratigraphic framework in the Cuddapah Basin, AP. *Geol. Surv. India Spec. Publ.*, 2001, **55**(2), 31–57.
18. Chandrakala, K., Pandey, O. P., Mall, D. M. and Sarkar, D., Seismic signatures of a Proterozoic thermal plume below southwestern part of Cuddapah Basin, Dharwar Craton. *J. Geol. Soc. India*, 2010, **76**, 565–572.
19. Chatterjee, N. and Bhattacharji, S., Petrology, geochemistry and tectonic settings of the mafic dikes and sills associated with the evolution of the Proterozoic Cuddapah Basin of south India. *Proc. Indian Acad. Sci. (Earth Planet. Sci.)*, 2001, **110**(4), 433–453.
20. Chakraborty, K., Mukhopadhyay, P. and Pankaj, P., Magmatism in western Cuddapahs: the mafic sills and lava flows of Vempalle and Tadpatri formations. *J. Geol. Soc. India*, 2016.
21. Srikanthia, S. V., Kuppapalle volcanic – a distinct upper Papagani volcanic activity in the Cuddapah basin. *J. Geol. Soc. India*, 1984, **25**(12), 775–779.
22. Downs, R., The RRUFF Project: an integrated study of the chemistry, crystallography, Raman and infrared spectroscopy of minerals.

- In Paper presented at the Program and Abstracts of the 19th General Meeting of the International Mineralogical Association, Kobe, Japan, 2006, O03–O13; <http://rruff.info/>
23. Groppo, C., Rinaudo, C., Cairo, S., Gastaldi, D. and Compagnoni, R., Micro-Raman spectroscopy for a quick and reliable identification of serpentine minerals from ultramafics. *Eur. J. Mineral.*, 2006, **18**, 319–329.
  24. Holland, T. J. B. and Powell, R., An improved and extended internally consistent thermodynamic dataset for phases of petrological interest, involving a new equation of state for solids. *J. Metamorph. Geol.*, 2011, **29**(3), 309–343.
  25. Connolly, J. A. D., Computation of phase equilibria by linear programming: a tool for geodynamic modeling and its application to subduction zone decarbonation. *Earth Planet. Sci. Lett.*, 2005, **236**, 524–541.
  26. <http://database.iem.ac.ru/mincryst>
  27. Speiler, A. R. and Bird, D. K., Epidote in geothermal systems. *Rev. Mineral. Geochem.*, 2004, **56**(1), 235–300; 10.2138/gsrng.56.1.235.
  28. Schroeder, T., Wolfgang, B., Niels, J., Svenja, J., Patrick, M. and Andreas, K., Fluid circulation and carbonate vein precipitation in the footwall of an oceanic core complex, Ocean Drilling Program Site 175, Mid-Atlantic Ridge. *Geochem., Geophys., Geosyst.*, 2015, **16**(1), 3716–3732; <https://doi.org/10.1002/2015GC006041>.
  29. Young-Joon, Lee, Morse, J. W. and Wiltschko, D. V., An experimentally verified model for calcite precipitation in veins. *Chem. Geol.*, 1996, **130**(3–4); [https://doi.org/10.1016/0009-2541\(96\)00008-3](https://doi.org/10.1016/0009-2541(96)00008-3).
  30. Chen, Y., Han, X., Wang, Y. and Lu, J., Precipitation of calcite veins in serpentinized harzburgite at Tianxiu hydrothermal field on Carlsberg Ridge (3.67°N), Northwest Indian Ocean: implications for fluid circulation. *J. Earth Sci.*, 2020, **31**(1), 91–101.
  31. Saha, D., Chakraborty, S. and Tripathy, V., Intracontinental thrusts and inclined transpression along eastern margin of the East Dharwar Craton, India. *J. Geol. Soc. India*, 2010, **75**, 323–337.
  32. Tripathy, V. and Saha, D., Inversion of calcite twin data, paleo-stress reconstruction and multi-phase weak deformation in cratonic interior – evidence from the Proterozoic Cuddapah Basin, India. *J. Struct. Geol.*, 2015, **77**, 62–81.
  33. Geology and Mineral Resources of India. Geological Survey of India, Miscellaneous Publication No. 30, 2010, part XXII.

ACKNOWLEDGEMENTS. We thank Shri K. Chandrasekhar (former Director), Petrology Division, Geological Survey of India (GSI), Southern Region, Hyderabad for encouragement and support throughout the study. We also thank Dr Santanu Bhattacharya (Director, GSI, Southern Region) for taking keen interest in analysing many of the petrographic sections at the EPMA laboratory of GSI, Dr Sessa Sai (GSI, Nagpur) for logistic help during fieldwork, and reviewer whose constructive comments helped improve the manuscript.

Received 20 April 2020; revised accepted 3 January 2022

doi: 10.18520/cs/v122/i7/826-839